

On the origin of critical nematic fluctuations in pnictide superconductors

S.-F. Wu,^{1,2,3,*} W.-L. Zhang,¹ L. Li,⁴ H. B. Cao,⁵ H.-H. Kung,¹
A. S. Sefat,⁴ H. Ding,^{2,3,6} P. Richard,^{2,3,6,†} and G. Blumberg^{1,7,‡}

¹*Department of Physics and Astronomy, Rutgers University, Piscataway, NJ 08854, USA*

²*Beijing National Laboratory for Condensed Matter Physics,*

and Institute of Physics, Chinese Academy of Sciences, Beijing 100190, China

³*School of Physical Sciences, University of Chinese Academy of Sciences, Beijing 100190, China*

⁴*Materials Science & Technology Division, Oak Ridge National Laboratory, Oak Ridge, TN 37831*

⁵*Neutron Scattering Division, Oak Ridge National Laboratory, Oak Ridge, TN 37831*

⁶*Collaborative Innovation Center of Quantum Matter, Beijing, China*

⁷*National Institute of Chemical Physics and Biophysics, 12618 Tallinn, Estonia*

(Dated: December 19, 2017)

We employ polarization-resolved Raman spectroscopy to study critical nematic fluctuations in $\text{Ba}(\text{Fe}_{1-x}\text{Au}_x)_2\text{As}_2$ superconductors above and across well separated tetragonal to orthorhombic phase transition at temperature $T_S(x)$ and the Néel transition at $T_N(x)$. The static Raman susceptibility in XY symmetry channel increases upon cooling from room temperature following the Curie-Weiss law, with Weiss temperature $T_\theta(x)$ several tens of degrees lower than $T_S(x)$. Data reveals a hidden nematic quantum critical point at $x_c = 0.031$ when the system becomes superconducting, indicating a direct connection between quantum critical nematic fluctuations and unconventional superconductivity. We attribute the origin of the nematicity to charge quadrupole fluctuations due to electron transfer between the nearly degenerate d_{xz}/d_{yz} orbitals.

It is widely believed that the interactions leading to high-temperature superconductivity are already present in the parent compounds. The parent compounds of the Fe-based superconductors usually show a tetragonal to orthorhombic structural transition at temperature T_S that is accompanied by transition into collinear antiferromagnetic phase at temperature T_N , typically only slightly lower than T_S .

Recently, much attention was devoted to studies of non-symmetric dynamical fluctuations above T_S which break local four-fold symmetry, usually referred as nematic fluctuations [1]. Below T_S , significant anisotropy was found for properties measured along the two planar orthogonal Fe-Fe directions, notably in electrical resistivity [2], optical conductivity [3], thermopower [4], and local density-of-states (DOS) [5]. It has been established both by the static probes such as shear modulus C_{66} [6–9], Young’s modulus Y_{110} [10, 11], the elastoresistance coefficient m_{66} [12, 13], and by the dynamic probe: polarization resolved Raman scattering [14–22], that the underlying nematic fluctuations have a distinct XY quadrupole symmetry and that they extend to temperatures far above T_S . However, the origin of the nematic fluctuations remains under debate.

Among interpretations, it has been proposed that the fluctuations could originate from charge transfer between degenerate d_{xz}/d_{yz} orbitals [16, 23–30], or from magnetic interactions [31–38]. We noticed that for $\text{Ba}(\text{Fe}_{1-x}\text{Au}_x)_2\text{As}_2$ superconductors the T_S and T_N transition temperatures are well separated, thus the system

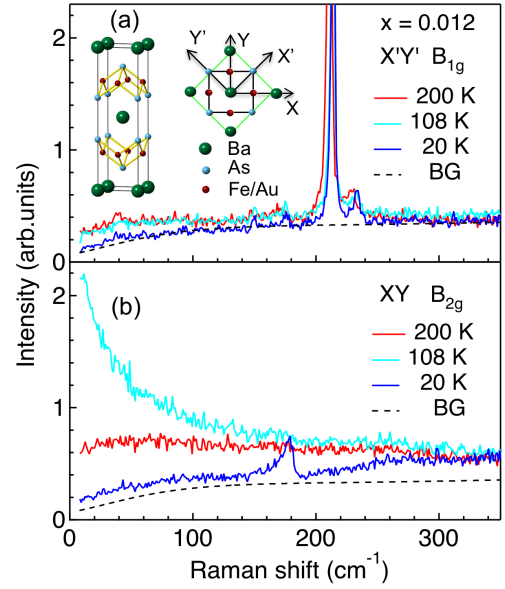


FIG. 1. Crystal structure of $\text{Ba}(\text{Fe}_{1-x}\text{Au}_x)_2\text{As}_2$ and the definition of X , Y , X' and Y' directions are shown in the top panel. The green and black lines represent 4-Fe and 2-Fe unit cells, respectively. (a) and (b) Secondary emission for $X'Y'$ and XY polarizations, correspondingly. The dashed lines show background at 20 K determined by intensity in $X'Y'$ polarization.

provides a platform to study separately the charge and spin contributions to the nematic fluctuations.

In this Letter, we use the static Raman susceptibility derived from the dynamical response acquired in the XY -symmetry quadrupole channel to study the evolution of the nematic fluctuations above and across the

* sfwu@iphy.ac.cn

† pierre.richard.qc@gmail.com

‡ girsh@physics.rutgers.edu

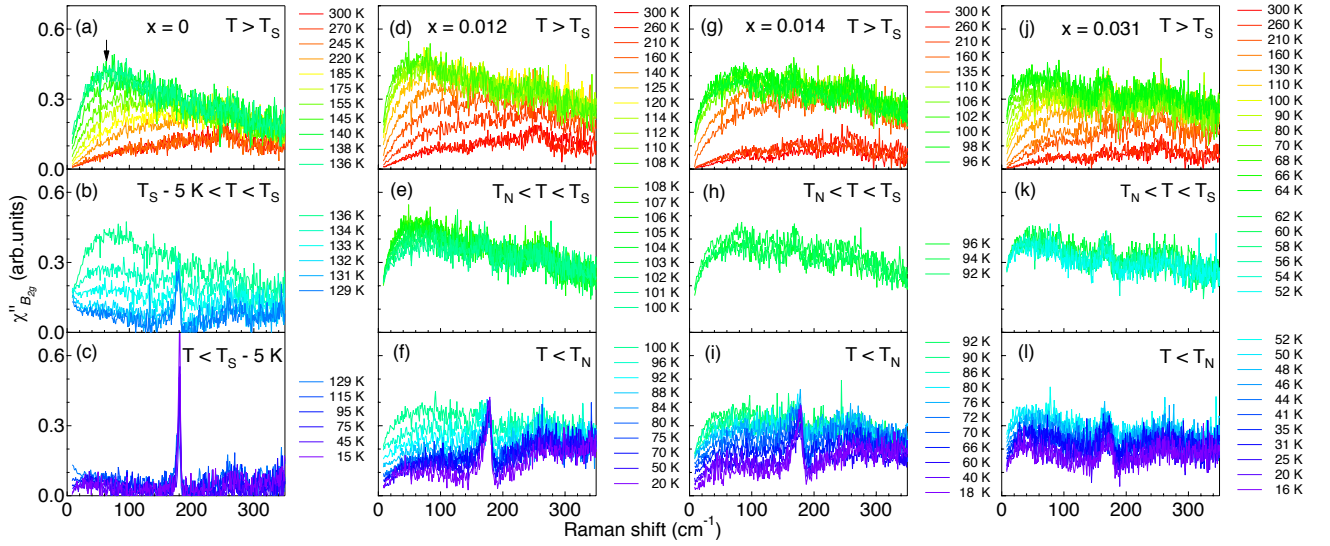


FIG. 2. Temperature dependence of the Raman response $\chi''_{B_{2g}}(\omega, T, x)$ for $\text{Ba}(\text{Fe}_{1-x}\text{Au}_x)_2\text{As}_2$. (a)-(c) $x = 0$, (d)-(f) $x = 0.012$, (g)-(i) $x = 0.014$ and (j)-(l) $x = 0.031$. The arrow in (a) indicates the QEP.

structural and magnetic phase transitions as function of Au doping into $\text{Ba}(\text{Fe}_{1-x}\text{Au}_x)_2\text{As}_2$ crystals. Above T_S , the static Raman susceptibility follows the Curie-Weiss law with Weiss temperature $T_\theta(x)$ about 40-60 K lower than T_S . The growth of susceptibility stops below T_S , when degeneracy of the d_{xz} and d_{yz} orbitals is lifted, emphasizing a relation between nematicity and d_{xz}/d_{yz} quadrupole charge/orbital fluctuations. Furthermore, we demonstrate that the charge quadrupole moment is monotonically increasing with Au doping while the ordered magnetic moment is decreasing with the doping, indicating that the charge quadrupole fluctuations and stripe magnetic orders are competing. Moreover, the data reveal a hidden quantum critical point at critical doping x_c defined by $T_\theta(x_c) = 0$, which appears to be at the very heart of the superconducting dome. Below T_N , the susceptibility decreases rapidly upon cooling as the magnetic order parameter develops and as a spin-density-wave (SDW) gap is depleting the DOS of the occupied d_{xz}/d_{yz} orbitals.

Single crystals of $\text{Ba}(\text{Fe}_{1-x}\text{Au}_x)_2\text{As}_2$ ($x = 0, 0.012,$

$0.014, 0.031$) were grown out of self-flux using a high-temperature solution growth technique described in Refs. [41, 42], and the chemical compositions were determined by energy dispersive spectroscopy (EDS) analysis. The room-temperature crystal structure, illustrated in the inset of Figs. 1(a), belongs to space group $I4/mmm$ (point group D_{4h}). The T_S and T_N of the Au-doped samples were determined, respectively, by the temperature evolution of the neutron nuclear and the magnetic Bragg peak intensities shown in Figs. 3(f)-3(h). For the pristine compound, $T_S \simeq T_N = 135$ K, as was determined by bulk property measurements [42], in agreement with neutron diffraction measurements [43]. The T_S and T_N values for the compositions studied are summarized in Table I.

The crystals used for Raman scattering were cleaved and positioned in a continuous helium flow optical cryostat. The measurements were performed in a quasi-back scattering geometry along the crystallographic c -axis using the Kr^+ laser line at 647.1 nm (1.92 eV). The excitation laser beam was focused into a $50 \times 100 \mu\text{m}^2$ spot on the ab -surface, with the incident power around 10 mW. The scattered light was collected and analyzed by a triple-stage Raman spectrometer designed for high-stray light rejection and throughput, and then recorded using a liquid nitrogen-cooled charge-coupled detector. Raman scattering intensity data were corrected for the spectral responses of the spectrometer and detector. The laser heating in the Raman experiments is determined by imaging the appearance of stripes due to twin domain formation at the structural phase transition temperature T_S [17]. When stripes appear under laser illumination, the spot temperature is just slightly below T_S , thus $T_S = kP + T_{\text{cryo}}$, where T_{cryo} is the temperature

TABLE I. Summary of the structural and magnetic phase transition temperatures determined by neutron scattering [Figs. 3(f)-3(h)], Weiss temperature T_θ (K), ordered magnetic moment and charge quadrupole moment $Q(x)$ for $\text{Ba}(\text{Fe}_{1-x}\text{Au}_x)_2\text{As}_2$ samples.

Sample	T_S (K)	T_N (K)	T_θ (K)	$M(\mu_B)$	$Q(x)$ (arb.units)
$x=0$	135	135	96 ± 4	0.87 [39]	5.7 ± 0.2
$x=0.012$	108	100	64 ± 4	0.50 ± 0.02 [40]	6.7 ± 0.3
$x=0.014$	96	92	46 ± 8	0.42 ± 0.04 [40]	6.7 ± 0.5
$x=0.031$	63	54	4 ± 5	0.36 ± 0.02 [40]	7.5 ± 0.3

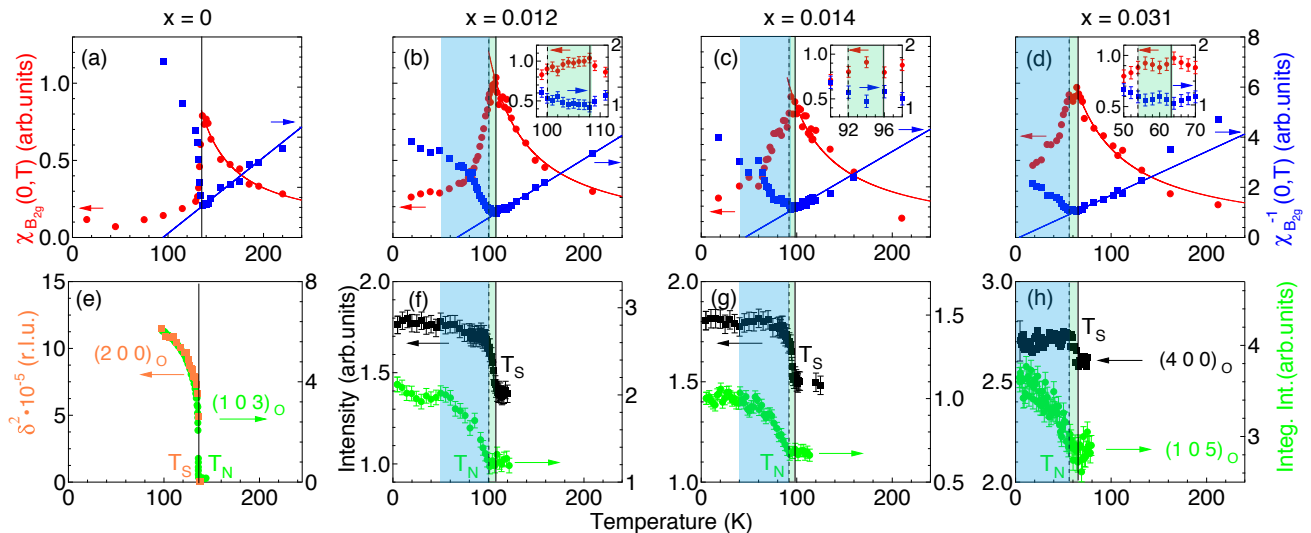


FIG. 3. (a)-(d) Temperature dependence of the static Raman susceptibility $\chi_{B_{2g}}(0, T, x)$ (red solid circles) and its inverse $\chi_{B_{2g}}^{-1}(0, T, x)$ (blue solid square) at different doping concentrations x . The red and blue curves are fits to the Curie-Weiss law (a linear function for inverse susceptibility). The solid lines mark $T_S(x)$, whereas the dashed lines mark $T_N(x)$. The insets in (b)-(d) are zoom-in around the transition temperatures. (e) Temperature dependence of δ^2 (orange solid squares) deduced from the splitting of the $(2\pm\delta\ 0\ 0)$ nuclear Bragg peak of BaFe_2As_2 , from Ref. [43], with $\delta^2 = (a+b)/(a-b)$ representing the orthorhombicity of a crystal with in-plane lattice parameters a and b . The green solid circles represent the temperature evolution of the integrated intensity of the $(1\ 0\ 3)$ magnetic Bragg peak, from Ref. [43]. (f)-(h) Temperature evolution of the $(2\ 0\ 0)$ nuclear Bragg peak intensity (black solid squares) and of the $(1\ 0\ 5)$ magnetic Bragg peak intensity (green solid circles) for $\text{Ba}(\text{Fe}_{1-x}\text{Au}_x)_2\text{As}_2$ in the orthorhombic phase [40].

of cold helium gas in the cryostat, P is the laser power and k is the heating coefficient. By recording T_{cryo} when the stripes appear at different laser powers, we can deduce the heating coefficient using a linear fit: $k = 1 \pm 0.1$ K/mW.

We define X and Y directions along the 2-Fe unit cell basis vectors (at 45° from the Fe-Fe direction) in the tetragonal phase, whereas X' and Y' are along the Fe-Fe directions, as shown in the inset of Fig. 1(a). According to Raman selection rules, the XX , XY , $X'X'$, $X'Y'$ scattering geometries probe $A_{1g} + B_{1g}$, $A_{2g} + B_{2g}$, $A_{1g} + B_{2g}$ and $A_{2g} + B_{1g}$ symmetry excitations of the D_{4h} point group respectively. The data in the $X'Y'$ (B_{1g}) symmetry channel barely changes with temperature [Fig. 1(a)]. In contrast, the spectrum in the XY (B_{2g}) symmetry channel show strong temperature dependence [Fig. 1(b)]. Therefore, we subtract the background signal recorded in the $X'Y'$ geometry from the data measured in the XY geometry to obtain $\chi''_{B_{2g}}(\omega, T)$ response function [14].

In Figs. 2(a)-2(c), we show the Raman response for BaFe_2As_2 in the B_{2g} channel at temperatures between 300 K and 15 K. The most remarkable feature appearing upon cooling is a quasi-elastic peak (QEP) that reaches its maximum intensity around T_S/T_N [Fig. 2(a)]. The QEP is sharply suppressed within 5 K below T_S/T_N [Fig. 2(b)] and it vanishes at lower temperatures [Fig. 2(c)]. Above $T_S(x)$, the Raman response for the Au-doped samples ($x = 0.012, 0.014, 0.031$) shows similar behav-

ior as for the pristine compound [Figs. 2(d), 2(g) and 2(j)]. Unlike for the pristine compound, $T_S(x) \neq T_N(x)$ in the doped samples. Interestingly, the passage across $T_S(x)$ does not affect the Raman response significantly, as shown in Figs. 2(e), 2(h) and 2(k). The situation is quite different when temperature decreases below $T_N(x)$ [Figs. 2(f), 2(i) and 2(l)]. As with the pristine compound, the QEP is suppressed quickly upon cooling below $T_N(x)$.

For better understanding of QEP evolution in the B_{2g} channel, we compute the static nematic susceptibility $\chi_{B_{2g}}(0, T, x)$ from the experimental data using the Kramers-Kronig transformation [14, 19, 20]:

$$\chi_{B_{2g}}(0, T, x) \approx \frac{2}{\pi} \int_0^{350 \text{ cm}^{-1}} \frac{\chi''_{B_{2g}}(\omega, T, x)}{\omega} d\omega. \quad (1)$$

The integrand underlines importance of Raman response in low-frequency limit. We use linear extrapolation for response below 8 cm^{-1} instrumental cut-off.

In Figs. 3(a)-3(l), we show temperature dependence of $\chi_{B_{2g}}(0, T, x)$. Above $T_S(x)$, the static Raman susceptibility is well described by the Curie-Weiss law

$$\chi_{B_{2g}}(0, T, x) \propto Q^2(x)/(T - T_\theta(x)), \quad (2)$$

where $T_\theta(x)$ is the Weiss temperature and square of the charge quadrupole moment $Q^2(x)$ is proportional to Curie constant [22]. This fit is better expressed by the linear behavior of the inverse susceptibility, $\chi_{B_{2g}}^{-1}(0, T, x)$.

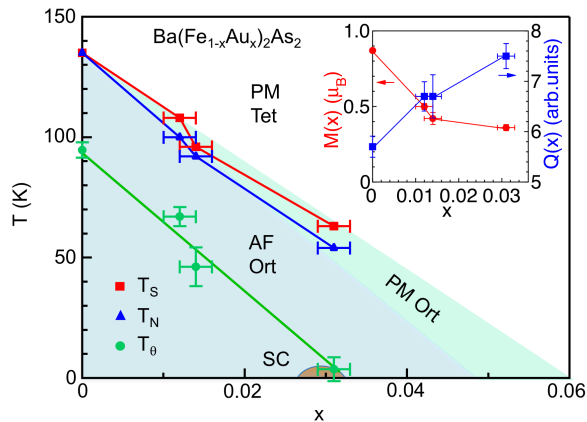


FIG. 4. Phase diagram of $\text{Ba}(\text{Fe}_{1-x}\text{Au}_x)_2\text{As}_2$. Red solid squares and blue solid triangles represent $T_S(x)$ and $T_N(x)$, respectively. The green solid circles denote interpolated Weiss temperature $T_\theta(x)$. The inset shows the doping dependence of the ordered magnetic moment $M(x)$ and charge quadrupole moment $Q(x)$.

The values of $T_\theta(x)$, which correspond to the abscissae of the linear fits, are given in Table I and shown in Fig. 4 [44].

$T_\theta(x)$ is monotonically decreasing function of x , at about 40-60 K lower than $T_S(x)$. At a critical doping $x_c = 0.031$ the Weiss temperature approaches zero, indicating a hidden quantum critical point. At this critical Au-doping concentration the system is a superconductor with $T_c = 2.5$ K [42], indicating a strong connection between quantum critical nematic fluctuations and unconventional superconductivity [2, 45].

For pristine BaFe_2As_2 , susceptibility $\chi_{B_{2g}}(0, T, x = 0)$ is rapidly suppressed just below T_S/T_N . In contrast, for the Au-doped samples, $\chi_{B_{2g}}(0, T, x > 0)$ has a plateau-like saturation between split $T_S(x)$ and $T_N(x)$, with only a slight decrease, followed by much faster decrease below $T_N(x)$ to a saturation value at temperature coinciding with magnetic order parameter saturation temperature, Figs. 3(e)-3(h).

The fact that the static susceptibility stops increasing on cooling below T_S , when T_N is lower than T_S , indicates that the origin of the critical fluctuations is not magnetic but rather is driven by the charge quadrupole fluctuations [19, 20, 22]. The likely scenario for quadrupole charge fluctuations with B_{2g} symmetry is a charge transfer between the nearly degenerate d_{xz} and d_{yz} orbitals. Such quadrupole charge fluctuations are expected to slow down below T_S , when the degeneracy of d_{xz}/d_{yz} orbitals is lifted, and be suppressed below T_N , when the SDW gap depletes the electronic DOS at the Fermi level, with

complete suppression when the magnetic ordering is fully established.

In more details, the electron transfer between quasi-degenerate d_{xz}/d_{yz} orbitals induces a charge quadrupole moment $Q(x)$ proportional to the local charge imbalance $n_{xz} - n_{yz}$. The charge quadrupole moment can be estimated from the fitted Curie constant, Eq. (2). The $Q(x)$ values for $\text{Ba}(\text{Fe}_{1-x}\text{Au}_x)_2\text{As}_2$ are summarized in Table I. In the inset of Fig. 4, we show the doping dependence of $Q(x)$ and of the ordered magnetic moment $M(x)$ as a function of Au concentration x . The opposite doping dependence of the charge quadrupole moment $Q(x)$ and of the magnetic moment $M(x)$ suggests that the charge quadrupole order at the Fe site competes with stripe magnetic order. Same conclusion can be reached from the fact that the static XY quadrupole susceptibility saturates at T_S and is gradually suppressed below T_N as the stripe magnetic order parameter builds up.

In conclusion, we studied nematic Raman response for Au-doped BaFe_2As_2 samples, which have split structural and magnetic transition temperatures. The data revealed that above T_S the static Raman susceptibility in the quadrupole B_{2g} channel follows a Curie-Weiss behavior. Between T_S and T_N , the susceptibility stops increasing, and it decreases only below T_N , when the magnetic order parameter develops and a SDW gap opens. We attribute the corresponding increase of the Raman susceptibility to quadrupole charge fluctuations due to electron transfer between nearly degenerate d_{xz} and d_{yz} orbitals. Weiss temperature $T_\theta(x)$ extrapolated from the high-temperature fluctuations is decreasing with doping concentration x and is several tens of degrees lower than $T_S(x)$ and $T_N(x)$. Importantly, the critical concentration x_c defining the quantum critical point $T_\theta(x_c) = 0$ is located inside the small superconducting dome, thus underlining the role played by the quadrupole orbital fluctuations in the pairing mechanism of the Fe-based superconductors [2, 45]. The extrapolated charge quadrupole moment $Q(x)$ is monotonically increasing function, while the ordered magnetic moment $M(x)$ is a decreasing function of x , suggesting that the charge quadrupole order competes with the collinear antiferromagnetic order.

The spectroscopic research at Rutgers was supported by the US Department of Energy, Basic Energy Sciences, and Division of Materials Sciences and Engineering under Grant No. DE-SC0005463. The sample growth and characterization at ORNL was supported by the US Department of Energy, Basic Energy Sciences, Materials Sciences and Engineering Division. Work at IOP was supported by grants from NSFC (11674371 and 11274362) and MOST (2015CB921301, 2016YFA0401000 and 2016YFA0300300) of China.

[1] E. Fradkin, S. A. Kivelson, M. J. Lawler, J. P. Eisenstein, and A. P. Mackenzie, “Nematic Fermi fluids in condensed

matter physics,” *Annu. Rev. Condens. Matter Phys.* **1**,

- 153 (2010).
- [2] J.-H. Chu, J. G. Analytis, K. De Greve, P. L. McMahon, Z. Islam, Y. Yamamoto, and I. R. Fisher, "In-plane resistivity anisotropy in an underdoped iron arsenide superconductor," *Science* **329**, 824 (2010).
 - [3] A. Dusza, A. Lucarelli, F. Pfner, J.-H. Chu, I. R. Fisher, and L. Degiorgi, "Anisotropic charge dynamics in detwinned $\text{Ba}(\text{Fe}_{1-x}\text{Co}_x)_2\text{As}_2$," *EPL* **93**, 37002 (2011).
 - [4] S. Jiang, H. S. Jeevan, J. K. Dong, and P. Gegenwart, "Thermopower as a sensitive probe of electronic nematicity in iron pnictides," *Phys. Rev. Lett.* **110**, 067001 (2013).
 - [5] E. P. Rosenthal, E. F. Andrade, C. J. Arguello, R. M. Fernandes, L. Y. Xing, X. C. Wang, C. Q. Jin, A. J. Millis, and A. N. Pasupathy, "Visualization of electron nematicity and unidirectional antiferroic fluctuations at high temperatures in NaFeAs ," *Nat. Phys.* **10**, 225 (2014).
 - [6] T. Goto, R. Kurihara, K. Araki, K. Mitsumoto, M. Akatsu, Y. Nemoto, S. Tatematsu, and M. Sato, "Quadrupole effects of layered iron pnictide superconductor $\text{Ba}(\text{Fe}_{0.9}\text{Co}_{0.1})_2\text{As}_2$," *J. Phys. Soc. Jpn.* **80**, 073702 (2011).
 - [7] M. Yoshizawa, D. Kimura, T. Chiba, S. Simayi, Y. Nakanishi, K. Kihou, C. Lee, A. Iyo, H. Eisaki, M. Nakajima, and S. Uchida, "Structural quantum criticality and superconductivity in iron-based superconductor $\text{Ba}(\text{Fe}_{1-x}\text{Co}_x)_2\text{As}_2$," *J. Phys. Soc. Jpn.* **81**, 024604 (2012).
 - [8] M. Yoshizawa and S. Simayi, "Anomalous elastic behavior and its correlation with superconductivity iron-based superconductors $\text{Ba}(\text{Fe}_{1-x}\text{Co}_x)_2\text{As}_2$," *Mod. Phys. Lett. B* **26**, 1230011 (2012).
 - [9] R. Kurihara, K. Mitsumoto, M. Akatsu, Y. Nemoto, T. Goto, Y. Kobayashi, and M. Sato, "Critical slowing down of quadrupole and hexadecapole orderings in iron pnictide superconductor," *J. Phys. Soc. Jpn.* **86**, 064706 (2017).
 - [10] A. E. Böhmer, P. Burger, F. Hardy, T. Wolf, P. Schweiss, R. Fromknecht, M. Reinecker, W. Schranz, and C. Meingast, "Nematic susceptibility of hole-doped and electron-doped BaFe_2As_2 iron-based superconductors from shear modulus measurements," *Phys. Rev. Lett.* **112**, 047001 (2014).
 - [11] A. E. Böhmer and C. Meingast, "Electronic nematic susceptibility of iron-based superconductors," *C. R. Physique* **17**, 90 (2016).
 - [12] H. H. Kuo, J. H. Chu, J. C. Palmstrom, S. A. Kivelson, and I. R. Fisher, "Ubiquitous signatures of nematic quantum criticality in optimally doped Fe-based superconductors," *Science* **352**, 958 (2016).
 - [13] J. H. Chu, H. H. Kuo, J. G. Analytis, and I. R. Fisher, "Divergent nematic susceptibility in an iron arsenide superconductor," *Science* **337**, 710 (2012).
 - [14] Y. Gallais, R. M. Fernandes, I. Paul, L. Chauvière, Y.-X. Yang, M.-A. Méasson, M. Cazayous, A. Sacuto, D. Colson, and A. Forget, "Observation of incipient charge nematicity in $\text{Ba}(\text{Fe}_{1-x}\text{Co}_x)_2\text{As}_2$," *Phys. Rev. Lett.* **111**, 267001 (2013).
 - [15] P. Massat, D. Farina, I. Paul, S. Karlsson, P. Strobel, P. Toulemonde, M.-A. Méasson, M. Cazayous, A. Sacuto, S. Kasahara, T. Shibauchi, Y. Matsuda and Y. Gallais, "Charge induced nematicity in FeSe ," *Proc. Natl. Acad. Sci. USA* **113**, 9177 (2016).
 - [16] Y. Gallais and I. Paul, "Charge nematicity and electronic Raman scattering in iron-based superconductors," *C. R. Physique* **17**, 113 (2016).
 - [17] F. Kretzschmar, T. Böhm, U. Karahasanović, B. Muschler, A. Baum, D. Jost, J. Schmalian, S. Caprara, M. Grilli, C. Di Castro, J. G. Analytis, J.-H. Chu, I. R. Fisher and R. Hackl, *Nat. Phys.* **12**, 560 (2016).
 - [18] T. Böhm, R. Hosseinian Ahangharnejhad, D. Jost, A. Baum, B. Muschler, F. Kretzschmar, P. Adelman, T. Wolf, H.-H. Wen, J.-H. Chu, I. R. Fisher, and R. Hackl, "Superconductivity and fluctuations in $\text{Ba}_{1-p}\text{K}_p\text{Fe}_2\text{As}_2$ and $\text{Ba}(\text{Fe}_{1-n}\text{Co}_n)_2\text{As}_2$," *Physica Status Solidi (b)* **254**, 1600308 (2017).
 - [19] V. K. Thorsmølle, M. Khodas, Z. P. Yin, Chenglin Zhang, S. V. Carr, Pengcheng Dai, and G. Blumberg, "Critical quadrupole fluctuations and collective modes in iron pnictide superconductors," *Phys. Rev. B* **93**, 054515 (2016).
 - [20] W. L. Zhang, P. Richard, H. Ding, A. S. Sefat, J. Gillett, S. E. Sebastian, M. Khodas, and G. Blumberg, "On the origin of the electronic anisotropy in iron pnictide superconductors," *arXiv:1410.6452* (2014).
 - [21] U. F. Kaneko, P. F. Gomes, A. F. García-Flores, J.-Q. Yan, T. A. Lograsso, G. E. Barberis, D. Vaknin, and E. Granado, "Nematic fluctuations and phase transitions in LaFeAsO : A Raman scattering study," *Phys. Rev. B* **96**, 014506 (2017).
 - [22] W.-L. Zhang, S.-F. Wu, S. Kasahara, T. Shibauchi, Y. Matsuda, and G. Blumberg, "Stripe quadrupole order in the nematic phase of $\text{FeSe}_{1-x}\text{S}_x$," *arXiv:1710.09892* (2017).
 - [23] S. Onari and H. Kontani, "Self-consistent vertex correction analysis for iron-based superconductors: Mechanism of coulomb interaction-driven orbital fluctuations," *Phys. Rev. Lett.* **109**, 137001 (2012).
 - [24] T. Kontani, H. Saito and S. Onari, "Origin of orthorhombic transition, magnetic transition, and shear-modulus softening in iron pnictide superconductors: Analysis based on the orbital fluctuations theory," *Phys. Rev. B* **84**, 024528 (2011).
 - [25] H. Kontani and Y. Yamakawa, "Linear response theory for shear modulus C_{66} and Raman quadrupole susceptibility: Evidence for nematic orbital fluctuations in Fe-based superconductors," *Phys. Rev. Lett.* **113**, 047001 (2014).
 - [26] H. Yamase and R. Zeyher, "Superconductivity from orbital nematic fluctuations," *Phys. Rev. B* **88**, 180502 (2013).
 - [27] F. Krüger, S. Kumar, J. Zaanen, and J. van den Brink, "Spin-orbital frustrations and anomalous metallic state in iron-pnictide superconductors," *Phys. Rev. B* **79**, 054504 (2009).
 - [28] W. C. Lv and P. Phillips, "Orbitally and magnetically induced anisotropy in iron-based superconductors," *Phys. Rev. B* **84**, 174512 (2011).
 - [29] E. Bascones, B. Valenzuela, and M. J. Calderin, "Magnetic interactions in iron superconductors: a review," *C. R. Physique* **17**, 36 (2016).
 - [30] M. Khodas and A. Levchenko, "Raman scattering as a probe of nematic correlations," *Phys. Rev. B* **91**, 235119 (2015).
 - [31] R. M. Fernandes, A. V. Chubukov, and J. Schmalian, "What drives nematic order in iron-based superconductors?" *Nat. Phys.* **10**, 97 (2014).

- [32] R. M. Fernandes, L. H. VanBebber, S. Bhattacharya, P. Chandra, V. Keppens, D. Mandrus, M. A. McGuire, B. C. Sales, A. S. Sefat, and J. Schmalian, “Effects of nematic fluctuations on the elastic properties of iron arsenide superconductors,” *Phys. Rev. Lett.* **105**, 157003 (2010).
- [33] R. M. Fernandes, A. V. Chubukov, J. Knolle, I. Eremin, and J. Schmalian, “Preemptive nematic order, pseudogap, and orbital order in the iron pnictides,” *Phys. Rev. B* **85**, 024534 (2012).
- [34] A. V. Chubukov, M. Khodas, and Rafael M. Fernandes, “Magnetism, superconductivity, and spontaneous orbital order in iron-based superconductors: Which comes first and why?” *Phys. Rev. X* **6**, 041045 (2016).
- [35] D. S. Inosov, “Spin fluctuations in iron pnictides and chalcogenides: From antiferromagnetism to superconductivity,” *C. R. Physique* **17**, 60 (2016).
- [36] U. Karahasanovic, F. Kretzschmar, T. Böhm, R. Hackl, I. Paul, Y. Gallais, and J. Schmalian, “Manifestation of nematic degrees of freedom in the Raman response function of iron pnictides,” *Phys. Rev. B* **92**, 075134 (2015).
- [37] A. Hinojosa, J. S. Cai, and A. V. Chubukov, “Raman resonance in iron-based superconductors: The magnetic scenario,” *Phys. Rev. B* **93**, 075106 (2016).
- [38] L. Classen, R.-Q. Xing, M. Khodas, and A. V. Chubukov, “Interplay between magnetism, superconductivity, and orbital order in 5-pocket model for iron-based superconductors: Parquet renormalization group study,” *Phys. Rev. Lett.* **118**, 037001 (2017).
- [39] P. C. Dai, “Antiferromagnetic order and spin dynamics in iron-based superconductors,” *Rev. Mod. Phys.* **87**, 855 (2015).
- [40] S.-F. Wu, W.-L. Zhang, L. Li, H. B. Cao, H.-H. Kung, A. S. Sefat, H. Ding, P. Richard, and G. Blumberg, “Anomalous magneto-elastic coupling in Au-doped BaFe_2As_2 ,” [arXiv:1712.01903](https://arxiv.org/abs/1712.01903) (2017).
- [41] A. S. Sefat, “Bulk synthesis of iron-based superconductors,” *Curr. Opin. Solid State Mater. Sci.* **17**, 59 (2013).
- [42] L. Li, H. B. Cao, M. A. McGuire, J. S. Kim, G. R. Stewart, and A. S. Sefat, “Role of magnetism in superconductivity of BaFe_2As_2 : Study of 5d Au-doped crystals,” *Phys. Rev. B* **92**, 094504 (2015).
- [43] S. D. Wilson, Z. Yamani, C. R. Rotundu, B. Freelon, E. Bourret-Courchesne, and R. J. Birgeneau, “Neutron diffraction study of the magnetic and structural phase transitions in BaFe_2As_2 ,” *Phys. Rev. B* **79**, 184519 (2009).
- [44] We note that the derived $T_\theta(x)$ and $Q(x)$ depend on the background subtraction. Here we used the $X'Y'$ background as a reference. The error bars for $T_\theta(x)$ are estimated from the fitting procedure.
- [45] S. Lederer, Y. Schattner, E. Berg, and S. A. Kivelson, “Enhancement of superconductivity near a nematic quantum critical point,” *Phys. Rev. Lett.* **114**, 097001 (2015).